Astrodynamics
https://mc03.manuscriptcentral.com/astrod

The Deepspace Multi-Object Orbit Determination System and its Application to Hayabusa2's Asteroid Proximity Operations

Hiroshi Takeuchi[1,2] (✉), Kent Yoshikawa[3], Yuto Takei[3], Yusuke Oki[3], Shota Kikuchi[1], Hitoshi Ikeda[3],Stefania Soldini[1,4], Naoko Ogawa[1], Yuya Mimasu[1], Go Ono[3], Fuyuto Terui[1], Naoya Sakatani[1], Manabu Yamada[5], Toru Kouyama[6], Shingo Kameda[7], Takanao Saiki[1], Yuichi Tsuda[1,2]

1 Institute of Space and Astronautical Science, Japan Aerospace Exploration Agency, Sagamihara, 252-5210, Japan

2 SOKENDAI (The Graduate University for Advanced Studies), Hayama, 240-0193, Japan

3 Research and Development Directorate, Japan Aerospace Exploration Agency, Sagamihara, 252-5210, Japan

4 University of Liverpool, Liverpool, UK L69 3BX, United Kingdom

5 Chiba Institute of Technology, Narashino, 275-0016, Japan

6 National Institute of Advanced Industrial Science and Technology, Koto-ku, 135-0064, Japan

7 Rikkyo University, Toshima-ku, 171-8501, Japan

(Hiroshi Takeuchi,takeuchi@isas.jaxa.jp)

Abstract: The Deepspace Multi-Object Orbit Determination System (DMOODS) is described and its usage in the asteroid proximity operation of the Hayabusa2 mission are presented. This system has been developed at JAXA for the primary purpose of determining the trajectory of deep-space spacecraft for JAXA's planetary missions. The weighted least squares batch filter is used for the orbit estimator of DMOODS. The orbit estimator supports more than 10 data types and some of them are used for relative trajectory measurements between multiple space objects including natural satellites and small bodies. This system is consisting of a set of computer programs running on Linux-based consumer PCs on the ground that are used not only for orbit determination itself but also used for data generation of radiometric tracking data such as Delta-DOR and Doppler tracking data. During the asteroid proximity phase of Hayabusa2, this system played essential roles in some operations for which very strict navigation requirements are imposed or operations in which few optical data were obtained due to special constraints on the spacecraft attitude or distance toward the asteroid. One of the examples is the orbit determination during the solar conjunction phase, in which the navigation accuracy is degraded by the effect of the solar corona. The big range bias caused by the solar corona was well estimated with DMOODS by the combination of LIDAR and ranging measurements in the superior solar conjunction phase of Hayabusa2. For the orbiting operations of Target-Markers and the MINERVA-II2 rover, a simultaneous estimation of six trajectories of four artificial objects and a natural object was made by DMOODS. This kind of simultaneous orbit determination of multi artificial objects in deepspace had never been done before in the history of humankind.

Keywords: Orbit Determination, Optical Navigation, Gravity Measurements, Superior Solar Conjunction, Delta-DOR

Nomenclature

BCRF	The Barycentric Celestial Reference Frame
DDOR	Delta Differential One-way Ranging
HP	Home Position
OD	Orbit Determination
c	Speed of light (m/s)
$p(x, y)$	brightness ($0 \sim 1$) of the pixel (x, y) of an on-board camera image
η	a model parameter of the thermal radiation model ($0 \sim 1$)
$\boldsymbol{e}, \dot{\boldsymbol{e}}$	Earth's position vector relative to the asteroid (km) and its time derivative (km/s)
$\boldsymbol{s}, \dot{\boldsymbol{s}}$	Sun's position vector relative to the asteroid (km) and its time derivative (km/s)
$\hat{\boldsymbol{x}}, \hat{\boldsymbol{y}}, \hat{\boldsymbol{z}}, \dot{\hat{\boldsymbol{x}}}, \dot{\hat{\boldsymbol{y}}}, \dot{\hat{\boldsymbol{z}}}$	x-, y-, and z-axis unit vector of the HP coordinate and those time derivatives
$\boldsymbol{Q}, \dot{\boldsymbol{Q}}$	rotation matrix from inertial frame (BCRF) to HP coordinate and its time derivative
a_j , ϵ_j	albedo and emissivity of an ith facet of a small body's shape model
A, B, C	solve-for parameters for the solar corona correction model (m)
R_s	radius of the Sun (= 696,000km) used in the solar corona correction model
ϕ_0	reference latitude (= 10°) used in the solar corona correction model
f	up-leg or down-leg carrier frequency (Hz)
$\bar{C}_{nm}, \bar{S}_{nm}$	normalized gravity coefficients of the degree n and order m

1 Introduction

The history of deep space orbit determination software in Japan dates back to early 1980s, when the first Japanese deepspace probes called Sakigake and Suisei aimed to encounter Halley's comet were launched in 1985. The software named ISSOP written in Fortran was jointly developed by the Institute of Space and Astronautical Science (ISAS) and Fujitsu Limited before their launches and successfully supported both probes [1]. The software have been gradually updated and continuously supported past Japanese deepspace probes since then.

In 2006, a development of another deep space orbit determination system, DMOODS, was started in order to support Delta-DOR technique, of which inter-agency standardization activities were started at the Consultative Committee for Space Data System (CCSDS) among NASA, ESA, and JAXA in the same year. Because the Delta-DOR technology require a high precision Earth station location modeling, Earth rotation modeling and media calibration capabilities, it adopted the latest modern models and conventions, for which the latest related parameters should be obtained on a daily basis and freely available via the Internet. Usages of such models in DMOODS are described in Section 2. The other features of new system include adoption of the object-oriented framework written in C++ and usages of nonproprietary libraries for whole system. A multithreaded processing is applied to some time-consuming calculations (e.g. hit-testing toward an asteroid shape model consisting of a large number of polygons) so that performance of the software can be maximized under modern multi-core based CPU environment. Most of data interfaces are based on the standards adopted by CCSDS and other internationally standardized or recommended information.

Initial development of the system was dedicated to Delta-DOR related software such as data correlation (both for Quasars and spacecraft) software and a priori value calculation software with precise modeling for wide and narrow VLBI(DOR) observables. The JAXA's first on-board DOR signal generator was experimentally developed as a dedicated instrument and installed to the IKAROS spacecraft launched in 2010. The use of DDOR observables for the orbit determination of IKAROS was demonstrated with the initial prototype of DMOODS. After the success of IKAROS, DOR signal functions were officially included to the JAXA's transponder and installed on-board the Hayabusa2 spacecraft. Part of the validated Delta-DOR related functions were transfered to ISSOP after being tested by the IKAROS mission, and a development of complete version of DMOODS started in 2013 toward the launch of Hayabusa2 in late 2014.

One of the difficult points in the navigation and guidance operation for Hayabusa2 was uncertainty in a priori

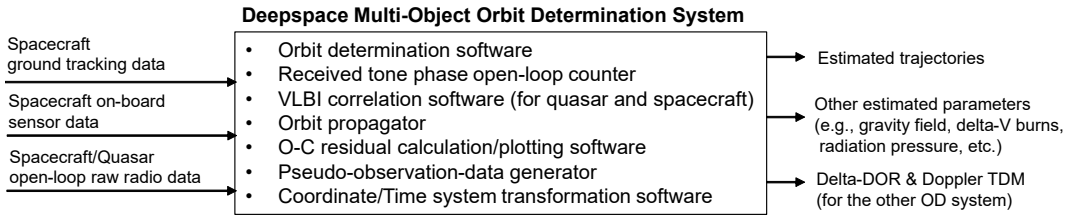

Fig. 1 Structural block diagram of DMOODS.

information of its trajectory. A priori orbit accuracy of Ryugu was very limited as a target of space exploration mission, because its closest approach distance to the Earth had been too far to be observed with ground-based radar measurements and its trajectory had estimated only with optical observations from the Earth before the launch of Hayabusa2. Because the orbit accuracy of Ryugu shall be improved during the approach phase of the Hayabusa2, simultaneous orbit determination function of spacecraft and its target object with on-board sensor observations was implemented to DMOODS. The orbit solutions of Ryugu generated by DMOODS were gradually updated in the approach phase of Hayabusa2 and the Ryugu's ephemeris had been regularly updated during the Ryugu proximity phase of Hayabusa2 [2–4]. Besides the generation of Ryugu's ephemeris, orbit solutions of DMOODS played essential role in the orbit insertion operations of Hayabusa2's Rover and Target Markers [5] and the post insertion observation operations of inserted orbiting objects because very precise orbit determination of Hayabusa2 and the orbiting objects were required for the estimation of gravity field of Ryugu. The usages of DMOODS for these operations and tentative estimation results of Ryugu's gravity field are described in Section 3.2. The DMOODS's solutions were also adopted in the post SCI escape operation [6] and solar conjunction phase operation [7], in which distance between Ryugu and Hayabusa2 were too long to be measured by LIDAR measurements and the quality of optical-based navigation were degraded. Therefore combination of radiometric data with optical data were important in these phases and DMOODS was used for generation of reference trajectories. The models used in the solar conjunction phase is described in Section 3.1.

2 Models and algorithms used in DMOODS

2.1 Observation data types

In this subsection measurement data types used in DMOODS are described. Table 1 lists the supported measurement types which include tracking station to spacecraft observables and observables between two space bodies. While data types that can be interfaced with CCSDS standard Tracking Data Message (TDM) are identified in the table, dedicated text-based formats are used for the other data types. DMOODS can read the TDM files generated by JAXA, NASA(DSN), and ESA(ESOC) as native format files. The definitions of measurement data types exchanged with the TDM files are described in [8].

The OP-NAV observable is defined as a direction (Right Ascension and Declination in inertial frame) to the center position of target's body from a spacecraft derived from an image taken with spacecraft's on-board camera. Distortion models of a camera are not included in orbit determination process but are applied in data pre-processing software in which Right Ascension and Declination of the target is calculated based on the spacecraft's attitude data, or by the position comparison between the target and background stars in the image. The Automated Image Tracking (AIT) data is a Hayabusa2's own data type which is a pixel information (X_{AIT} and Y_{AIT}) of the brightness center of an image taken by the on-board camera. The brightness center is calculated on the on-board processor so that image

Table 1 Measurement types supported by DMOODS. A check mark is placed in the second column (S-S) for the observables that are used to constrain relative trajectories of two space objects.

Data type	S-S	Description
1,2,3-way Doppler		TDM, received and transmitted frequencies
2-way Ranging		TDM, represented by range-unit (DSN) or second (JAXA and ESA)
DDOR(Quasar-SC)		TDM, sequential or same beam
DDOR(SC-SC)	✓	TDM, sequential or same beam (used between Hayabusa2 and PROCYON)
Az/El or RA/Dec		TDM, from a ground station to a space object
2-way LIDAR	✓	TDM, twice the distance between a SC and a body surface. using a target's shape model
SC to SC 2-way Range	✓	TDM, similar to LIDAR but no shape model is used and light time equation is solved
OP-NAV(RA/Dec)	✓	Direction to the target's centroid from a spacecraft with/without aberration correction
Automated Image Tracking (AIT)	✓	Direction to the brightness center of a image taken from a spacecraft
Relative state, position, or velocity	✓	relative states between two space bodies in a specific Cartesian coordinate system

data should not be transmitted to ground station but only compressed pixel information can be downlinked for the navigation. The observed values of AIT data are calculated on-board from an $N \times N$ pixel binary image of the target asteroid as follows:

$$X_{\mathrm{AIT}} = \sum_{x=1}^{N}\sum_{y=1}^{N} xp(x,y) \tag{1}$$

$$Y_{\mathrm{AIT}} = \sum_{x=1}^{N}\sum_{y=1}^{N} yp(x,y) \tag{2}$$

where $p(x,y)$ denotes the brightness (0 or 1) of the pixel (x,y) for the binarized image. For the calculation of computed values of AIT, a shape model of the target small body shall be used. Firstly solar incident angle toward each facet of the shape model is used for the calculation of the brightness of the facet, and it is binarized to 1 or 0 with a specified threshold level. The hit-tests from a spacecraft position to all facets are made and an averaged brightness center position is computed in each iteration of the OD process. For compatibility reasons there is another calculation mode in which no binarization is made but the calculated brightness of each facet is directly used in the calculation of a brightness center. The Relative state, position, and velocity data types are virtual observables which are defined as if a direct measurement of a relative state(six-dimensional relative positions and velocities), relative 3D position, or relative 3D velocity between two space objects are made in a specific Cartesian coordinate system. In the case of navigation of Hayabusa2, Ryugu's Home Position (HP) coordinate (defined in [5]), Ryugu's body-fixed coordinate, and Hayabusa2's body fixed coordinate are frequently used as coordinate system of those observables. A 6-dimensional (or 3-dimensional) covariance error matrix represented in these coordinate system is specified for each relative state (or relative position/velocity) observable, and it is transformed to the inertial frame to be used as a part of no-diagonal weighting matrix for the OD process. A transformation matrix from BCRF to HP coordinate, $\boldsymbol{Q}$, and its time derivative are derived in the followings. From the definition of the HP coordinate, $\hat{\boldsymbol{x}}, \hat{\boldsymbol{y}}, \hat{\boldsymbol{z}}$ are given by

$$\hat{\boldsymbol{z}} = \frac{\boldsymbol{e}}{|\boldsymbol{e}|} \tag{3}$$

$$\hat{\boldsymbol{x}} = \frac{\boldsymbol{p}}{|\boldsymbol{p}|}, \boldsymbol{p} = \boldsymbol{s} - \hat{\boldsymbol{z}}(\boldsymbol{s}\cdot\hat{\boldsymbol{z}}) \tag{4}$$

$$\hat{\boldsymbol{y}} = \hat{\boldsymbol{z}} \times \hat{\boldsymbol{x}} \tag{5}$$

with an auxiliary vector $\boldsymbol{p}$ and vectors $\boldsymbol{e}$ and $\boldsymbol{s}$ which are derived from planetary ephemeris. The transformation

matrix $\boldsymbol{Q}$ is written by

$$\boldsymbol{Q} = \begin{pmatrix} \hat{\boldsymbol{x}}^{\mathrm{T}} \\ \hat{\boldsymbol{y}}^{\mathrm{T}} \\ \hat{\boldsymbol{z}}^{\mathrm{T}} \end{pmatrix}. \tag{6}$$

and its time derivative $\dot{\boldsymbol{Q}}$ can be derived from $\dot{\hat{\boldsymbol{x}}}, \dot{\hat{\boldsymbol{y}}}, \dot{\hat{\boldsymbol{z}}}$ written by

$$\dot{\hat{\boldsymbol{z}}} = \frac{|\boldsymbol{e}|^2\dot{\boldsymbol{e}} - (\dot{\boldsymbol{e}}\cdot\boldsymbol{e})\boldsymbol{e}}{|\boldsymbol{e}|^3} \tag{7}$$

$$\dot{\hat{\boldsymbol{x}}} = \frac{|\boldsymbol{p}|^2\dot{\boldsymbol{p}} - (\dot{\boldsymbol{p}}\cdot\boldsymbol{p})\boldsymbol{p}}{|\boldsymbol{p}|^3} \tag{8}$$

$$\dot{\boldsymbol{p}} = \dot{\boldsymbol{s}} - \dot{\hat{\boldsymbol{z}}}(s\cdot\hat{\boldsymbol{z}}) - \hat{\boldsymbol{z}}(s\cdot\dot{\hat{\boldsymbol{z}}} + \dot{s}\cdot\hat{\boldsymbol{z}}) \tag{9}$$

$$\dot{\hat{\boldsymbol{y}}} = \dot{\hat{\boldsymbol{z}}}\times\hat{\boldsymbol{x}} + \hat{\boldsymbol{z}}\times\dot{\hat{\boldsymbol{x}}} \tag{10}$$

with an auxiliary vector $\dot{\boldsymbol{p}}$ and vectors $\dot{\boldsymbol{e}}$ and $\dot{\boldsymbol{s}}$ which are also derived from planetary ephemeris. From pattern matching between a camera image of an asteroid and its shape model, a relative position observable in the asteroid fixed coordinate can be derived. In such cases asteroid's rotation parameters might be estimated as solve-for parameters.

2.2 Force Model

2.2.1 Planetary Ephemeris

The planetary ephemeris used in DMOODS is based on a binary file in which Chebyshev coefficients for the Sun, planets and other bodies are included. The barycentric position, velocity, and acceleration of registered bodies at a given time (in TDB) can be derived from the ephemeris. The Chebyshev coefficients stored in DMOODS ephemeris can be diverted from ascii files provided as JPL Ephemeris files, or generated by re-sampling positions and velocities from the given CCSDS Orbit Ephemeris Message (OEM) files with specified number of Chebyshev coefficients and interval periods for each minor body. For Hayabusa2 mission, coefficients of the JPL DE430 are diverted for major bodies and long term trajectories for the other minor bodies were obtained from the JPL's HORIOZONS system and re-sampled with the specified number of Chebyshev coefficients and interval periods shown in Table 2 so that propagation error can be minimized even for a long term propagation of Ryugu as shown in [3].

Table 2 Minor bodies registered in the DMOODS's ephemeris for Hayabusa2 mission in addition to the DE430 bodies with the specified number of Chebyshev coefficients(n) per coordinate, and interval period(δt) in days.

Body	n	δt [days]	Body	n	δt [days]	Body	n	δt [days]
Ceres	11	8	Hygiea	13	16	Sylvia	11	16
Pallas	15	4	Eunomia	11	16	Thisbe	11	16
Juno	13	8	Psyche	11	8	Davida	11	16
Vesta	11	16	Amphitrite	11	16	Interamnia	11	16
Hebe	11	16	Europa	11	16	Ryugu *	13	2
Iris	11	16	Cybele	11	16	Ryugu †	13	2

2.2.2 Occultation Model

For the orbiter around small bodies, a shape model of the small body in STL format can be specified in order to detect the exact solar eclipse timings and calculate shadow function for the solar radiation pressure acting on the orbiting body. In orbit propagator, separation angle between the Sun and the small body is checked at each integration step and if the angle becomes smaller than the sum of maximum angular radius of small body and angular radius of the Sun, then hit-tests from the orbiter toward subdivided surface areas of the Sun are made. Program users can specify

*a priori solution from HORIZONS
†latest solution by DMOODS that has been regularly updated during the asteroid proximity phase

the number of the subdivisions, that is typically set to 100 to 200 so that about 1% accuracy is obtained during partial or annular eclipse. DMOODS also supports conventional shadow model in which a circular shape with specified radius of the occulting body is assumed (See Montenbruck [9]).

2.2.3 Thermal Radiation Pressure Model

Radiation pressure caused by thermal radiation and reflection of sunlight from the surface of a small body can be calculated with a shape model of the small body in DMOODS.Our proposed model is a modification of conventional earth radiation pressure model, e.g.,in Eq. (3.137) of Montenbruck [9].

In our model, Poynting vector $\boldsymbol{P}_i^{\mathrm{SB}}$ incident on an ith plate of a spacecraft plate model is summed up from $j(j = 1...., N)$ individual terms, corresponding to radiation from different facets of the shape model with area of dA_j

$$\boldsymbol{P}_i^{\mathrm{SB}} = \sum_{j=1}^{N} \left\{ \left(\nu_j a_j \cos\theta_j^{\mathrm{Sun}} + \frac{\eta(1-\nu_j)+\nu_j}{2(1+\eta)} \epsilon_j \right) dA_j \cos\theta_j^{\mathrm{SC}} \frac{\Phi_r}{\pi} \arctan^2\left(\frac{1}{r_{ij}}\right) \right\} \boldsymbol{e}_j^i \tag{11}$$

where ν_j is the visibility function of the facet j with respect to the sunlight, i.e. ν_j is equal to 1 at the day side and 0 at the night side, a_j and ϵ_j are albedo and emissivity of the facet j respectively, θ_j^{Sun} and θ_j^{SC} are the angles from the normal vector of facet j to the Sun direction and spacecraft direction respectively. Note that this sum runs only for the facets which are visible from the spacecraft, i.e., only if $\theta_j^{\mathrm{SC}} < \frac{\pi}{2}$ if the shape model is convex. The Φ_r is the solar flux at the distance r from the Sun where the small body locates, which obey the inverse square law. The Φ_r is assumed to be 1366 Wm^{-2} at 1AU in DMOODS despite it is suggested that the most accurate value to date is 1361 Wm^{-2} in [10]. The unit vector $\boldsymbol{e}_j^i$ points from the jth facet to the ith plate of the spacecraft, while the distance is r_{ij}. Note that this model can be used as an approximate model even if $r_{ij} \simeq 0$ because this equation does not diverge to infinity at $r_{ij} = 0$. The model parameter η is the night to day radiation ratio which takes a value between 0 and 1. This parameter has a relation with the thermal inertia of the small body. The zero thermal inertia corresponds to $\eta = 0$, implying non-zero thermal-infrared emission from the night side of the body. On the other hand, infinite thermal inertia corresponds to $\eta = 1$. Care must be taken that infrared radiation from the night side is constant, not depending on the longitude, in this simple model. It should be replaced by more realistic model if more accurate analysis is required.

2.2.4 Gravity Models

Currently DMOODS supports four gravity field models such as point-mass Newtonian model, point-mass relativistic model (defined in eq.(4-26) of Moyer [11]), spherical harmonics model, and the finite body direct integration model (Fukushima 2017 [12]). It is possible to automatically change the gravity model as a function of the distance between the gravity source and affected body in a single orbit arc, or to manually set individual model per orbit arc. While each model has own model parameters which can be estimated or considered, all models have 'GM' of the body as a common global parameter which can be estimated or considered across the different gravity models. The results of application of DMOODS for the estimation of Ryugu's gravity field with spherical harmonics model is described in Section 3.2.

2.3 Earth platform parameters and media calibration models

The Earth rotation models, Earth station location models (including tidal correction), and atmospheric propagation delay models on radio-wave frequency region used in DMOODS are all based on the IERS Conventions (2010) [13] or more newer updated version of it. The latest earth orientation parameters and their prediction files are regularly fetched from the IERS website and used as native input files of DMOODS. The JAXA's ground station coordinates

[‡] are represented by piece-wise linear model as a function of time in the ITRF2008 reference frame in order to represent co-seismic and post-seismic motion caused by a big earthquake in 2011 (Fig.2). The publicly available DSN station locations are based on the ITRF93 and they were transformed to ITRF2008 by a pre-processing program in DMOODS. The coordinates of ESA stations in the ITRF2008 reference frame were provided by ESOC.

Vienna Mapping Functions 3 (VMF3) [14] is used for the troposphere delay calibration model of DMOODS. The latest values of station-wise coefficients and their prediction files for JAXA and DSN stations calculated from Numerical Weather Models (NWMs) by the European Centre for Medium-Range Weather Forecasts (ECMWF) are regularly downloaded from the website and used as native input files of DMOODS. These hydrostatic and wet horizontal gradients (GRAD) are also included in the files [15] and used in DMOODS. No station-wise coefficients are provided for ESA stations and the empirical GPT3 [14] model is used for them.

For ionospheric propagation delay calibration, time series of line of sight Slant Total Electron Content (STEC) from each DSN complex toward target spacecrafts are calculated by DSN using the Global Ionospheric Model Calibration software (GIMCAL) [16] based on the spacecraft's predicted trajectories in OEM files provided from JAXA flight dynamics team. They are regularly provided from DSN to JAXA in TDM files and can be used as native input files of DMOODS.

The solar corona calibration model used in DMOODS is based on eq.(10-64) of Moyer [11], which is supported by the theory of Muhleman and Anderson [17]. In this model there are three solve-for parameters which should be estimated for each solar conjunction phase. The results of application of this model to the conjunction phase of Hayabusa2 is described in Section 3.1.

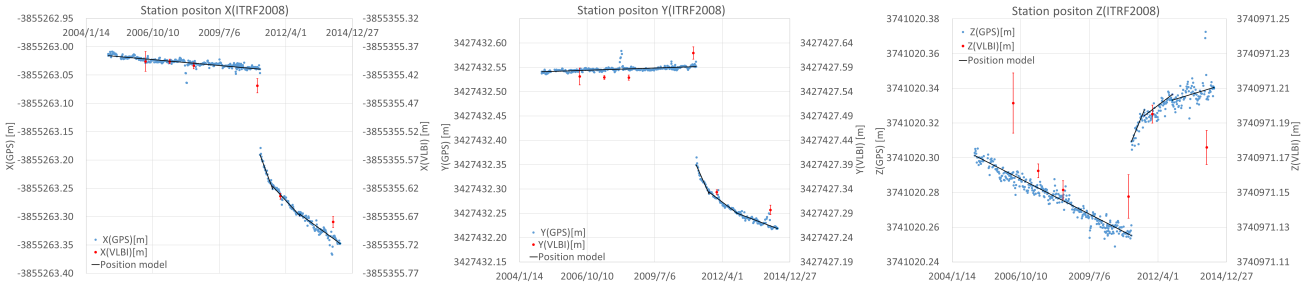

Fig. 2 Time series of station coordinates of the Usuda 64-m antenna and the IGS reference point at Usuda in ITRF2008 reference frame

3 Use of DMOODS in the Hayabusa2's Asteroid Proximity Operation

During the Hayabusa2's asteroid proximity phase, the main role of DMOODS was maintenance of Ryugu's ephemeris [3]. Utilizing the good accuracy of Doppler measurements and precise knowledge on Ryugu's inertial velocity is a key strategy for Hayabusa2's home position keeping operation and touch-down operations toward the surface of Ryugu, because a 2-way Doppler measurement from an Earth station to the spacecraft gives a direct measure of very precise descent velocity of Hayabusa2 toward Ryugu under the assumption that inertial velocity of Ryugu is known very precisely. Therefore JAXA-DSN mixed baseline Delta-DOR measurements were intensively carried out during the proximity period in order to maintain the Ryugu's ephemeris as accurate as possible. The Quasi-kinematic orbit determination method [18] with simultaneous three baseline Delta-DOR measurements played a vital role for the orbit determination.

[‡]Available on https://ddor.nav.isas.jaxa.jp/station_coordinates/ (cited 15 Jan 2020)

Additionally, DMOODS played vital roles in some situations where no LIDAR data could be used or quality of optical navigation data was degraded when the distance between Ryugu and Hayabusa2 was too long, or for the operations in which ultimate OD accuracy was requested for scientific reasons. Navigation results in such operations are described in the following subsections.

3.1 Navigation during superior solar conjunction phase

As described in [7] Hayabusa2 experienced a superior solar conjunction phase in November to December 2018, during which time JAXA's OD solutions calculated with DMOODS were frequently provided. During conjunctions the signals between a spacecraft and ground station pass through the solar corona surrounding the Sun. The free electrons in the plasma cause a positive group delay on Ranging and Delta-DOR measurements, and cause a negative phase delay on Doppler measurements. In addition to such biases the data noise of these radiometric measurements are degraded significantly.

During the conjunction phase Hayabusa2 was entered into a low energy transfer trajectory from Ryugu for safety reasons and thus the LIDAR measurements were not available and the communication link was very limited due to the dense solar corona. Therefore large bias in radiometric Ranging measurements caused by solar corona shall be well calibrated in order to maintain a good navigation and guidance accuracy along the reference trajectory. Since Hayabusa2 has no capability of simultaneous two-way X- and Ka-band links, the Doppler and Range biases cannot be mitigated and the delay calibration depends upon the modeling of solar corona surrounding the Sun. We adopted the up-leg and down-leg excess path delay model for solar corona calibration from Eq.(10-64) of Moyer[11]:

$$\Delta_{\text{corona}} = \pm \left[A \left(\frac{R_s}{p} \right) F + B \left(\frac{R_s}{p} \right)^{1.7} \exp\left(- \left(\frac{\phi}{\phi_0} \right)^2 \right) + C \left(\frac{R_s}{p} \right)^5 \right] \left(\frac{2295 \times 10^6 \text{Hz}}{f} \right)^2 \text{m} \tag{12}$$

where

$$F = \frac{1}{\pi} \tan^{-1} \frac{\sqrt{r_{\text{sc}}^2 - p^2}}{p} + \frac{1}{\pi} \tan^{-1} \frac{\sqrt{r_{\text{st}}^2 - p^2}}{p} \tag{13}$$

which applies both for the up or down legs. For up-leg case r_{st} means the distance between the Sun and transmitting station at the transmitted time solved from light time equations, and for down-leg case it's for the receiving station. The p is the closest approach radius from the Sun to the up-leg or down-leg light pass calculated in the light time calculation and ϕ is the latitude of the closest point in the Sun's body fixed frame.

This model was included in DMOODS for the solar corona calibration of Ranging, Delta-DOR, and Doppler observables. For the Ranging and Delta-DOR observables the plus sign in Eq.12 is used in the computation of calculated values, and the minus sign for Doppler observables. An orbit determination arc was set from November 23 to December 29, 2018, in which a set of solar corona model parameters A, B, C was estimated with the estimations of inertial trajectories of both Hayabusa2 and Ryugu. The trajectory correction maneuvers performed during the period were estimated accordingly with an impulse delta-V model. Used observables in this arc are summarized in Table 3. LIDAR data were only obtained in the 1st day of the arc (Nov.23) when Hayabusa2 left Ryugu and the very last day (Dec 29) after Hayabusa2 came back to its home position. A relative state observable between Hayabusa2 and Ryugu in the HP coordinate was set in the first day based on the camera image and a priori information before the OD. Due to the limited communication link, AIT observables were only obtained sparsely in this period. On the other hand, angular accuracy of AIT observables in this period was relatively good because Ryugu's angular size was enough small and there was few shadow on Ryugu's surface because the sun-asteroid-spacecraft angle was almost zero in this phase.

In the deep conjunction period, five X/Ka tracking passes were assigned. While the X/Ka 2-way Doppler were

obtained in all five passes, X/Ka 2-way Ranging data were obtained only in two of the five passes. Also, eight Ka-band DDOR passes were assigned in order to demonstrate the benefit of higher frequency for dense plasma. Apart from the range correction from the solar corona model, a 2-way Range bias was estimated on each tracking pass with a constraint of 20m (2-way, 1σ).

Table 3 Observation data used for the OD in the conjunction phase

	2-way Doppler	2-way Range	Delta-DOR	AIT	2-way LIDAR	Relative state
Start	Nov.23	Nov.24	Nov.23	Nov.23	Nov.23	Nov.23
End	Dec.29	Dec.29	Dec.26	Dec.29	Dec.29	Nov.23
# of passes	34 (X/X:29, X/Ka:5)	22 (X/X:20, X/Ka:2)	14 (X:6 Ka:8)	N.A.	2	1
# of data points	10491	668	115(QSQ)	438	301	1
Post-fit residuals	8.423[mm/s]	0.8135[m]	1.589[nsec]	0.0408[deg]	3.404[m]	N.A.

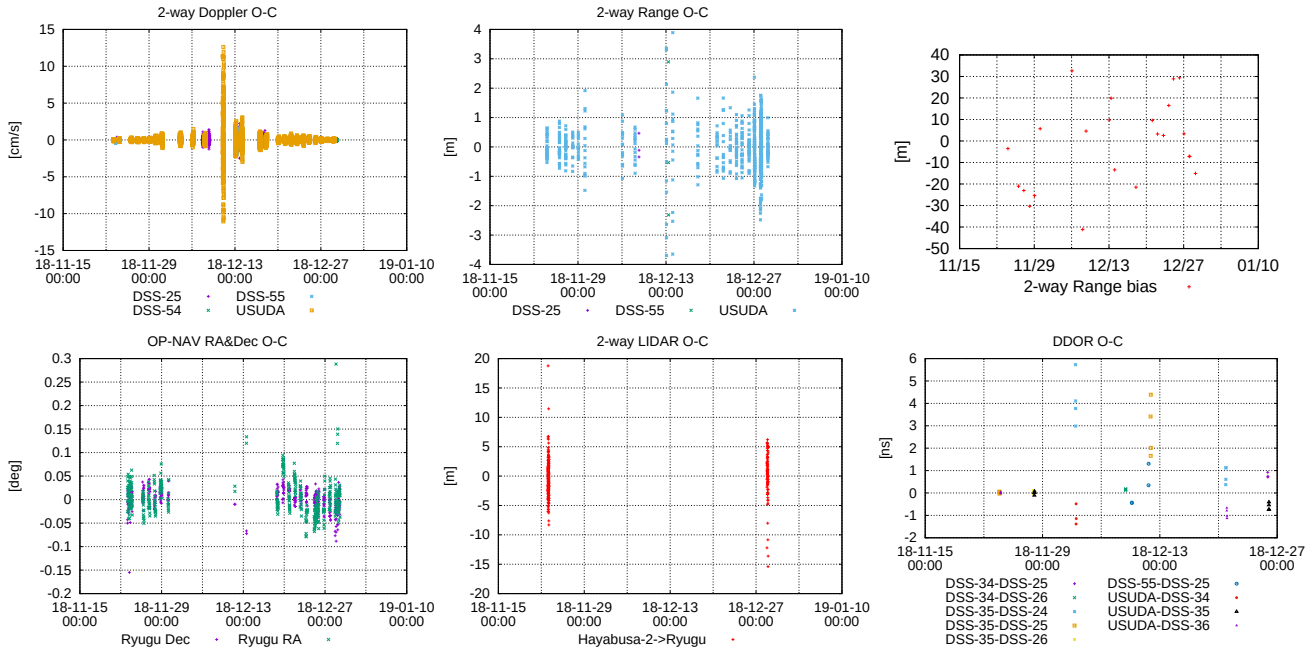

Fig. 3 Post-fit residuals of 2-way Doppler, 2-way Range, 2-way Range bias, AIT, 2-way LIDAR, and DDOR observables. A 2-way Range bias is estimated on each tracking pass (the upper right) independently from the global estimation of the solar corona delay.

Post-fit residuals of the observations are shown in Fig. 3. A large scattering due to the solar corona is obvious in the residuals of radiometric tracking data. Typical r.m.s values during normal periods are 0.1 mm/s for 2-way Doppler, and 50 pico-seconds for DDOR data. Especially, very big DDOR residuals ($\sim$ 6 nano seconds) were observed in the two Ka-band DDOR passes on December 2nd and December 11th. This is partially explained by the fact that the direction of Hayabusa2 from the Earth was near the Galactic center during this period, thus no usable strong quasars existed near Hayabusa2. The estimated values of A, B, C were, 99.898 [m], 5717.039 [m], 2.24 $\times$ 10^{-19} [m] respectively. The effect of the third term (represented by parameter C) was turned out to be negligible in our case. A time series of the estimated 2-way range bias component caused by the solar corona model corresponding to each 2-way Ranging point is plotted in Fig. 4. In the figure, contributions of the first and second terms (represented by parameter A and B), and the total delay bias are shown. The contribution of second term was decreased in the deep conjunction period because the latitude of the closest point became high in this period as shown in Fig. 5. It can be confirmed that the residuals of 2-way Range bias of each pass in Fig. 3 are almost scattered in a random manner.

We can conclude from this fact that the adopted solar corona model worked well for the solar conjunction period of Hayabusa2.

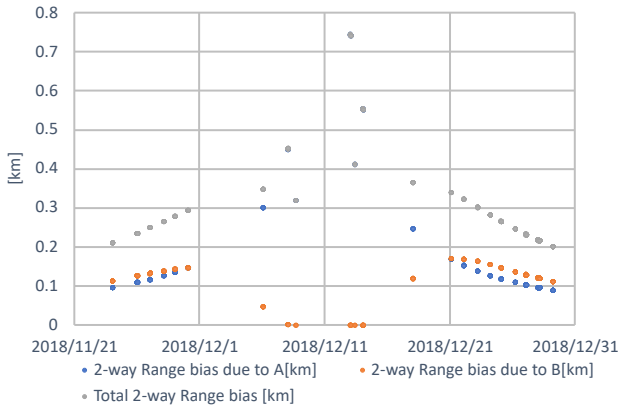

Fig. 4 Estimated 2-way solar corona bias, contribution of the first term (A), and the second term (B) for each ranging point. The smaller bias can be confirmed in two X/Ka tracks.

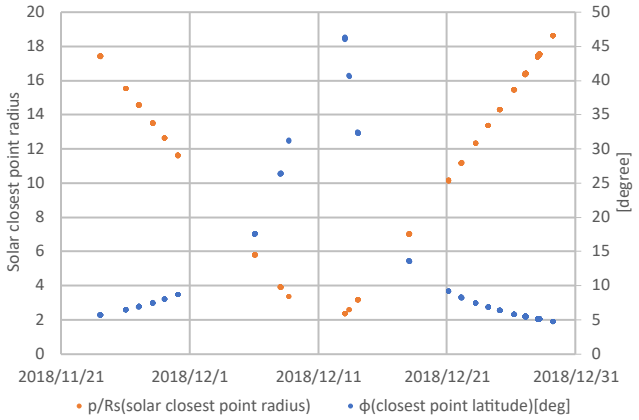

Fig. 5 The history of ϕ (sun-closest-point latitude) and p/Rs (sun-closest-point distance in solar radius unit) for each ranging point.

3.2 Target Markers and MINERVA-II2 orbiting operations

As described in [5], MINERVA-II2 rover was released from Hayabusa2 and inserted to the orbit around Ryugu in October 2nd, 2019. Two target markers (TM-E and TM-C) were also released from Hayabusa2 and inserted to an equatorial orbit (TM-E) and a polar orbit (TM-C) in September 17th, 2019. These operations require high navigation and guidance accuracy so that the orbiting objects are released at the right altitudes in order to be inserted to stable orbits [5]. After the separations there was also strict OD accuracy requirement in order to take images of orbiters as many as possible with the optical cameras onboard Hayabusa2. DMOODS was fully used everyday during these periods in order to satisfy the strict OD requirements.

After images of orbiting objects were successfully taken by the optical navigation camera telescope (ONC-T) onboard Hayabusa2 as shown in Fig. 6, the X/Y pixel positions of the orbiters were extracted and used for the orbit determination with a global estimation of spherical harmonics gravity of Ryugu. This was unique opportunity for Hayabusa2 mission to estimate the non-point-mass gravity field of Ryugu because gas-jet maneuvers are frequently inserted during the touch-down operations of Hayabusa2 and they are not suitable for precise gravity measurements.

Table 4 Obtained OP-NAV data

	Separation time	# of images (orbiting)	First image	Last image	# of images (separation)
TM-E	2019/9/16 16:17:40	39	2019/9/17 12:00:17	2019/9/19 4:30:26	35
TM-C	2019/9/16 16:24:20	49	2019/9/17 12:00:17	2019/9/19 19:00:26	35
MINERVA	2019/10/2 15:57:20	42	2019/10/3 1:53:24	2019/10/3 10:30:17	61

The configuration of the OD are shown in Fig. 7 and Fig. 8. Three relative state observables between Hayabusa2 and deployed objects in Hayabusa-2's body-fixed coordinate were set at the timings of their separations, i.e., the same positions and nominal separation velocity were assumed at the release epochs with the assumed a priori covariances error matrices. The obtained OP-NAV data are listed in Table 4. In addition to the orbiting images, many images are taken within a few minutes just after the separations. They have not yet used for the OD because exact positions of optical cameras and separated objects in Hayabusa2 body-fixed coordinate has not yet modeled in DMOODS,

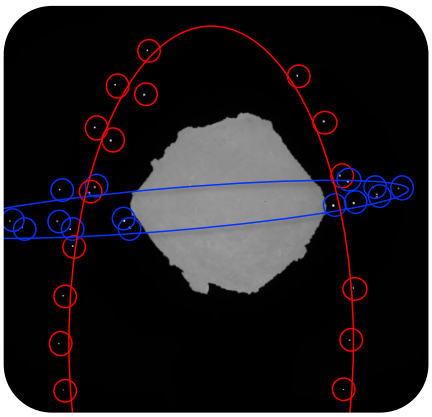

Fig. 6 The overlapped ONC-T images of orbiting TM-E and TM-C released from Hayabusa2 in September 17th, 2019. The identified TM-E positions and its orbit are drawn in red, and TM-C being drawn in blue. (Photo courtesy of JAXA, Chiba Institute of Technology, National Institute of Advanced Industrial Science and Technology, Rikkyo univ. Tokyo univ, Kochi univ, Nagoya univ, Meiji univ, and Aizu univ).

while all OP-NAV data generated from orbiting images are used for the OD. The LIDAR boresight direction in the spacecraft body-fixed frame is based on the values written in [19], and the camera distortion calibration model used in the OD is based on [20].

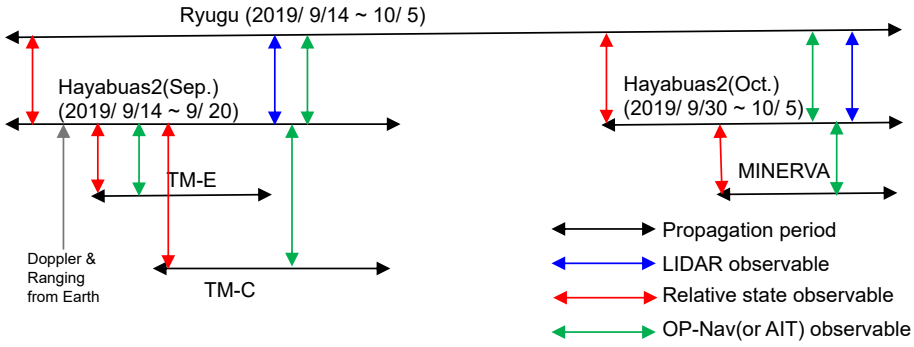

Fig. 7 Relationship of observables used in the OD.

As shown in the figures, six deepspace trajectories of four artificial objects and a natural object were simultaneously estimated with an estimation of Ryugu's gravity field. A priori (or initial) 8×8 spherical harmonics coefficients with a reference radius of 526m were calculated from a Ryugu's shape model assuming homogeneous density distribution. In order to constrain the estimation of coefficients we first assumed the empirical *Kaula rule* [21] as

$$\bar{C}_{nm}, \bar{S}_{nm} \approx \frac{K}{n^2} \tag{14}$$

where K is a scale factor dependent on the body size and shape. As discussed in [22], determining adequate value of K for small body is not a simple problem. Although we first assigned the values used in [22], $K = 0.087$ for zonal terms and $K = 0.025$ for other coefficients, but the OD was diverged with these values. Instead we first set the much smaller K such as 0.0001 to fix many other estimation parameters such as impulsive maneuvers of Hayabusa2, and after that the constraint was gradually relaxed iteratively. Because it was confirmed from the past LIDAR measurements that the X and Y components of center of mass of Ryugu is well coincident with the X and Y

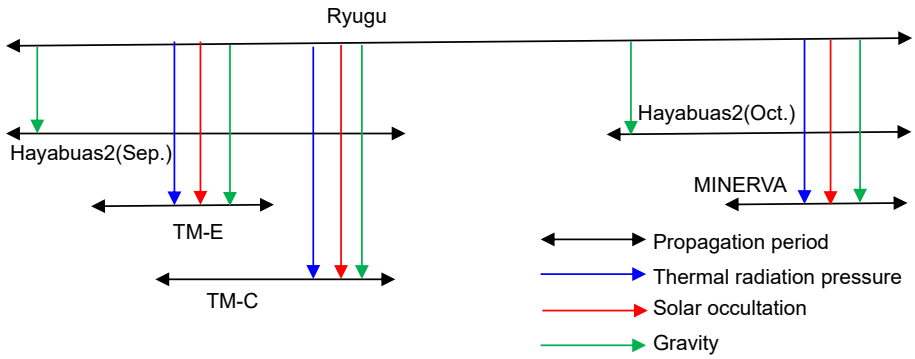

Fig. 8 Relationship of modeled forces acting on each object. Additionally, solar radiation pressure and gravity from the Sun and other planets affect all objects in the figure.

components of the origin of shape model, the corresponding terms $\bar{C}_{10}$ and $\bar{S}_{11}$ are binded to zero and not estimated. The radiation pressure model used for the orbiting objects is a simple cannonball model written as

$$\ddot{\boldsymbol{r}} = C_R \frac{A}{cM}(\boldsymbol{P}^{\mathrm{SB}} + \boldsymbol{P}^{\mathrm{Sun}}) \tag{15}$$

where $\boldsymbol{P}^{\mathrm{SB}}$ is the Poynting vector from the asteroid defined in Eq. 11 and $\boldsymbol{P}^{\mathrm{Sun}}$ is the Poynting vector from the Sun written as

$$\boldsymbol{P}^{\mathrm{Sun}} = \Phi_r \frac{\boldsymbol{r}}{|\boldsymbol{r}|} \tag{16}$$

where $\boldsymbol{r}$ is a sun-centered position vector of orbiting objects. For Hayabusa2, $\boldsymbol{P}^{\mathrm{SB}}$ is neglected and a more complex model is used for solar radiation pressure. The CCSDS Attitude Ephemeris Message (AEM) is a native format for the spacecraft attitude used in the solar radiation pressure model. The thermal properties of Ryugu assumed in this analysis are $a_j = 0.04$ and $\epsilon_j = 0.96$ for all facets of the shape model based on the values in [2]. The η has not changed from 0 in this work.

The observables used in this OD are summarized in Table 4, and post-fit residuals are shown in Fig. 9. A priori and estimated values of radiation pressure model parameters for the orbiting objects are summarized in Table 6.

Table 5 Observation data used for the OD

	2-way Doppler	2-way Range	OP-NAV(AIT)	2-way LIDAR	Relative State
Start	Sep.14	Sep. 14	Sep.14	Sep. 14	Sep. 16
End	Oct. 5	Oct. 4	Oct. 4	Oct. 2	Oct. 2
# of passes	23	16	N.A.	N.A.	N.A.
# of data points	33903	349	879	85183	5
Post-fit residuals (rms,1σ)	0.1777[mm/s]	0.9083[m]	0.1168[deg]	2.384[m]	N.A.

Table 6 Radiation pressure model parameters of orbiting objects

	C_R (a priori)	C_R (estimated)	Mass [kg]	Area [m^2]
TM-E	2.0	2.3068	0.29	$\pi(0.0504)^2$
TM-C	2.0	2.1936	0.29	$\pi(0.0504)^2$
MINERVA	1.113	0.9895	1.07	0.035

As shown in Fig. 9, the observation data were almost fitted but a few outliers remain in the OP-NAV residuals of low-altitude TM-C data. There are following potential issues to be investigated in order to improve the OD:

- Current scaling factor setting for the covariance matrix of gravity coefficients may not be optimized.

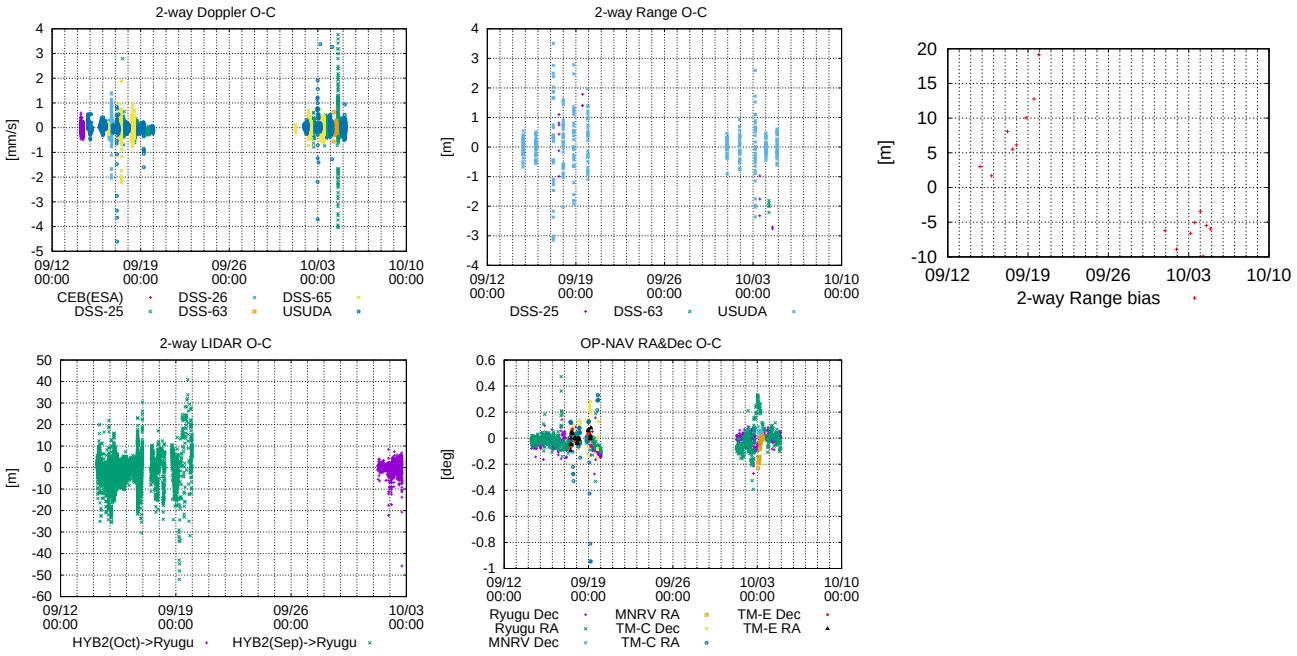

Fig. 9 Post-fit residuals of 2-way Doppler, 2-way Range, 2-way Range bias, 2-way LIDAR, and OP-NAV(AIT) observables in the Target Markers and MINERVA orbiting operations.

- Threshold parameters in AIT observation model may not been completely calibrated. This may be causing angular error when the shadow area on Ryugu is not small.
- Current distortion model used for the calibration of onboard cameras might be not well validated in the peripheral area of the image plane.
- Effect of thermal radiation is small in our case but there is a little improvement in the residuals by the adoption of the model. The model parameters may need to be changed to fit the data.
- The positions of onboard sensors (e.g. ONC-T or LIDAR) in spacecraft body-fixed coordinate have not yet modeled in DMOODS. Especially its modeling is a must to include the images taken just after separations.

If data are not fit even after the above points are solved, we may need to include experiential acceleration terms caused by unmodeled forces in the propagations of orbiters.

Tentative results of estimated gravity coefficients and GM are listed with a priori values in Table 7. Note that although all of the 8×8 updated coefficients are listed in the table, it is not clear about which terms are significantly updated from the a priori values by the limited number of observations. Further investigations are needed to evaluate it. In Fig. 10, the estimated gravity field and a priori gravity field are compared using the SHTOOLS software [23]. The three vector components of gravity field represented in spherical coordinate system and the total gravity disturbance on a sphere whose radius is equal to the reference radius of 526m are plotted for both cases.

4 Conclusions

The Deepspace Multi-Object Orbit Determination System is described. It was used for various operations in Hayabusa2's asteroid proximity phase. The effectiveness of the solar corona model implemented to DMOODS is validated with high reliability, because the Earth to spacecraft distances at the start and end timings of the OD arc are well determined

Table 7 The estimated values and a priori values of the normalized gravity coefficients of Ryugu. The estimated value of GM is 2.98751e-08 km^3s^{-2} while the a priori value is 3.00e-08 km^3s^{-2}.

n	m	$\bar{C}_{nm}$ (estimated)	$\bar{S}_{nm}$ (estimated)	$\bar{C}_{nm}$ (a priori)	$\bar{S}_{nm}$ (a priori)
0	0	1.000000000e+00	0.000000000e+00	1.000000000e+00	0.000000000e+00
1	0	−3.269214351e−08	0.000000000e+00	0.000000000e+00	0.000000000e+00
1	1	0.000000000e+00	0.000000000e+00	0.000000000e+00	0.000000000e+00
2	0	−2.483342581e−02	0.000000000e+00	−1.731946753e−02	0.000000000e+00
2	1	3.465777305e−05	−3.439282349e−05	−5.453175588e−05	−3.782742022e−04
2	2	−3.023548212e−03	−9.620037218e−04	−2.480064094e−03	−1.693767100e−03
3	0	6.504943454e−04	0.000000000e+00	6.631593187e−04	0.000000000e+00
3	1	2.827897830e−03	3.103027021e−03	2.712871801e−03	2.848850194e−03
3	2	1.474796017e−03	−8.117300275e−03	1.546370608e−03	−3.781793427e−03
3	3	8.855026414e−04	−2.247956239e−03	9.657256015e−04	−2.032447194e−03
4	0	1.180924805e−02	0.000000000e+00	7.517833147e−03	0.000000000e+00
4	1	2.152915157e−03	1.124009439e−03	2.277077457e−03	1.117540977e−03
4	2	−3.178656295e−04	1.841581078e−04	−3.201759127e−04	1.943513307e−04
4	3	−1.182457655e−04	−1.769174516e−04	−1.166784334e−04	−1.702196918e−04
4	4	−6.514036430e−04	−6.200271531e−05	−5.822426483e−04	−6.199423201e−05
5	0	1.673333075e−05	0.000000000e+00	1.672499546e−05	0.000000000e+00
5	1	4.587921161e−04	2.866657996e−04	4.546681280e−04	2.870040565e−04
5	2	6.402864251e−05	5.440236083e−04	6.413605579e−05	6.129817263e−04
5	3	−4.638029622e−04	8.496573844e−05	−4.623501624e−04	8.674208247e−05
5	4	−2.112525150e−04	−3.087302416e−04	−2.093671904e−04	−2.962237856e−04
5	5	−2.558760316e−06	−7.879390870e−05	−2.558972736e−06	−7.883871373e−05
6	0	−2.345425476e−03	0.000000000e+00	−2.119347824e−03	0.000000000e+00
6	1	−8.552238974e−04	4.906486161e−04	−8.839586228e−04	4.944181487e−04
6	2	−4.068551154e−04	−1.188917594e−04	−3.937316081e−04	−1.173144928e−04
6	3	−1.248191182e−04	2.867211358e−04	−1.252437058e−04	3.002984240e−04
6	4	−1.646341824e−05	1.077711954e−05	−1.647792969e−05	1.078879590e−05
6	5	5.122114274e−05	6.683717492e−05	5.114963620e−05	6.694386911e−05
6	6	3.215161674e−04	1.531750319e−04	3.194008023e−04	1.537786111e−04
7	0	−1.246904376e−04	0.000000000e+00	−1.242558419e−04	0.000000000e+00
7	1	2.045381145e−04	4.447971396e−04	2.048689107e−04	4.516520636e−04
7	2	2.002153821e−04	−3.377620286e−04	2.015826335e−04	−3.296677331e−04
7	3	2.768220116e−05	−1.547707274e−04	2.770573219e−05	−1.521657591e−04
7	4	−7.383911828e−05	−5.289432291e−05	−7.396758507e−05	−5.294760456e−05
7	5	−1.768856209e−04	7.229552787e−05	−1.775634964e−04	7.241176334e−05
7	6	2.141806525e−05	7.930154783e−07	2.140878250e−05	7.930131744e−07
7	7	−2.947060060e−05	1.457343508e−04	−2.948858891e−05	1.463397191e−04
8	0	9.488687214e−04	0.000000000e+00	9.034556298e−04	0.000000000e+00
8	1	2.312499863e−04	8.467260197e−05	2.322987773e−04	8.465693459e−05
8	2	−8.273162648e−05	5.192005490e−05	−8.301213285e−05	5.208054205e−05
8	3	1.514977525e−05	−1.066340392e−04	1.515698632e−05	−1.060714648e−04
8	4	−4.786682277e−05	2.506401032e−05	−4.784686161e−05	2.503806219e−05
8	5	7.109264176e−05	−6.674411589e−05	7.101606262e−05	−6.689885713e−05
8	6	−1.364086098e−04	−1.109849910e−04	−1.367017053e−04	−1.112523126e−04
8	7	6.867107949e−05	−1.189581227e−04	6.856541556e−05	−1.189821805e−04
8	8	3.404094193e−06	−1.561158676e−04	3.404371324e−06	−1.562890037e−04

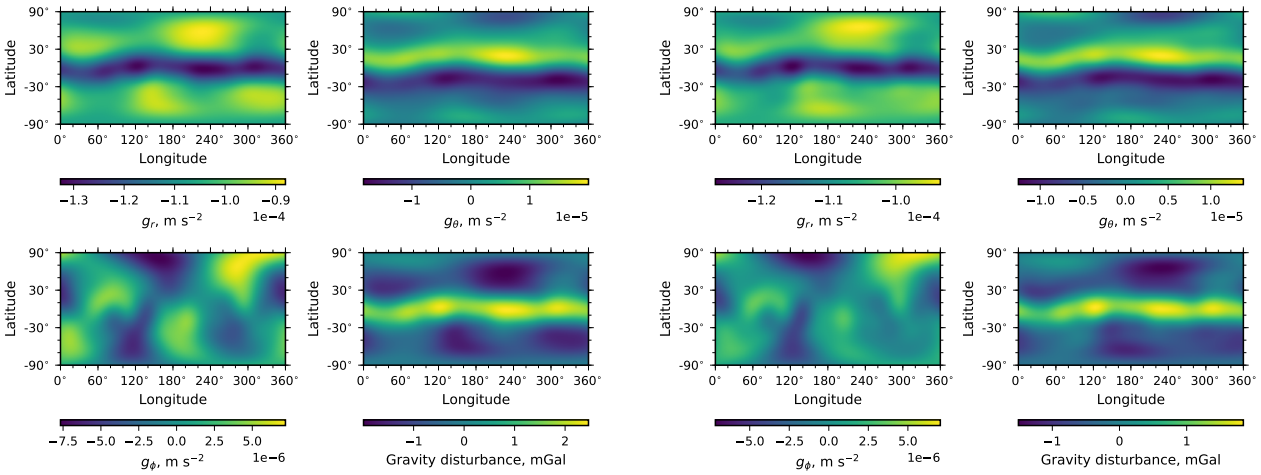

Fig. 10 The left four plots visualize the estimated gravity on the sphere at the reference radius and the right four plots visualize the a priori gravity on the same sphere.

through the LIDAR measurements from the spacecraft to asteroid. The six trajectories of four artificial objects and a natural object at a distance of more than 2 AU are simultaneously estimated by DMOODS. This kind of simultaneous orbit determination of multi artificial objects in deepspace had never been done in human history before.

Acknowledgements

This research was carried out at the Institute of Space and Astronautical Science (ISAS) of JAXA. The authors are grateful for the whole Hayabusa2 operation team for supplying the operation data used in this analysis. The authors would like to acknowledge the huge contribution made by the members of the Deepspacce Orbit Determination Group in ISAS: S. Taniguchi, N. Fujii, B. Ichikawa, T. Yagami, K. Takezawa, and M. Yoshikawa. Especially our special thanks to N. Fujii, who passed away too early on November 4, 2019 before the project was completed. Most of the tracking data from JAXA's deepspace stations were calibrated and distributed to the community by him. The authors would like to acknowledge the contribution from the Hayabusa2 navigation team in the Jet Propulsion Laboratory, California Institute of Technology (JPL), J. Bellerose, S. Bhaskaran, Z. B. Tarzi, and J. S. Border, for their excellent support to deliver the high quality navigation data from the Deep Space Network. We also acknowledge the contribution from the rest of the Hayabusa2 team in the JPL that provided various support in terms of the scheduling and technical assessment, including A. W. Kruger, S. Zadourian, M. A. Ritterbush, T. J. Hofmann, and S. W. Asmar. We also thank to the tracking team at the European Space Operations Centre (ESOC) of the ESA for the delivery of the Hayabusa2 tracking data from the European Space Tracking (ESTRACK) network. Finally, we are very thankful to two anonymous reviewers for the valuable comments that led to significant improvements of our paper.

References

[1] Nishimura T, Takano T, Yamada T, Kato T, Yano T. Tracking and orbit determination of 'SAKIGAKE' and 'SUISEI' encountering Halley's comet. In: Proceedings of the 15th International Symposium on Space Technology and Science, 1986: 1775–1780.

[2] Watanabe S, et al., Hayabusa2 arrives at the carbonaceous asteroid 162173 Ryugu - a spinning-top-shaped rubble pile, Science, 19 March, 2019, DOI:10.1126/science.aav8032

[3] Takeuchi H, et al., Simultaneous Orbit Determination of Hayabusa2 and Its Target Asteroid Ryugu (In preparation).

[4] Tsuda Y, et al., Guidance and Navigation Result of Hayabusa2 Asteroid Rendezvous Operation. *Astrodynamics*, 2020, (In this issue).
[5] Oki Y, Yoshikawa K, Takeuchi H, et al., Orbit Insertion Strategy of Hayabusa2 ' s Rover with The Large Release Uncertainty around Asteroid Ryugu. *Astrodynamics*, 2020, (In this issue).
[6] Saiki T, et al., Motion reconstruction of SCI. *Astrodynamics*, 2020, (In this issue).
[7] Soldini S, Takeuchi H, Taniguchi S, et al., Hayabusa2's Superior Solar Conjunction Mission. *Astrodynamics*, 2020, (In this issue).
[8] Navigation Data - Definitions and Conventions. Issue 3. Report Concerning Space Data System Standards (Green Book), CCSDS 500.0-G-3.3 Washington, D.C.:CCSDS, October 2016.
[9] Montenbruck O, Gill E. *Satellite Orbits: Models, Methods and Applications*, Springer Science & Business Media, 2000
[10] Kopp G, Lean J. L. A new, lower value of total solar irradiance: Evidence and climate significance. Geoph. Res. Lett., 38(1), L01,706, 2011
[11] Moyer T. D. *Formulation for Observed and Computed Values of Deep Space Network Data Types for Navigation*, Willy & Sons, New Jersey, 2003
[12] Fukushima T. Precise and Fast Computation of the Gravitational Field of a General Finite Body andIts Application to the Gravitational Study of Asteroid Eros, 2017, Astron. J., 154:145.
[13] Petit G, Luzum B (Eds.). IERS Conventions (2010), IERS Technical Note 36, 2010.
[14] Landskron D, Böhm J. VMF3/GPT3: Refined Discrete and Empirical Troposphere Mapping Functions, 2018, J Geod, 92: 349.
[15] Landskron D, Böhm J. Refined discrete and empirical horizontal gradients in VLBI analysis, J Geod 92, 1387-1399, 2018
[16] DSN Calibration and Modeling Services, DSN No.810-007, 104, Jet Propulsion Laboratory, 2018
[17] Muhleman D. O, Anderson, J. D. Solar wind electron densities from Viking dual-frequency radio measurements, Astrophysical Journal, Part 1, vol. 247, p. 1093-1101, 1981
[18] Takeuchi H, et al., A Quasi-Kinematic Orbit Determination Method for Deep Space Probes (In preparation).
[19] Noda H, Kunimori H, Mizuno T, et al. Laser link experiment with the Hayabusa2 laser altimeter for in-flight alignment measurement, Earth, Planets and Space, 69:2, 2017, doi: DOI 10.1186/s40623-016-0589-8.
[20] Suzuki H, Yamada M, Kouyama T, et al. Initial Inflight Calibration for Hayabusa2 Optical Navigation Camera (ONC) for Science Observations of Asteroid Ryugu. Icarus. 300, 2017.
[21] Kaula W. M. *Theory of Satellite Geodesy*, Blaisdell Publishing Company,Waltham,Massachusetts, 1966
[22] McMahon J, Scheeres D. J, Farnocchia D, Chesley S. Understanding Kaula's Rule for Small Bodies, American Geophysical Union, Fall Meeting 2015, abstract id.P41C-2084.
[23] Wieczorek M. A, Matthias M. SHTools - Tools for working with spherical harmonics, Geochemistry, Geophysics, Geosystems, 19, 2574-2592, 2018, doi:10.1029/2018GC007529.

Author biography

Please supply the photo, one-paragraph introduction (study experience, research interests, awards received, etc.), email address of each author of the work.